Incorporating latent hardening in visco-plastic self-consistent framework for performing texture simulations

Mirtunjay Kumar, Amit Singh, Vikrant Kumar Beura & Sumeet Mishra

Published online: 12 Jul 2021.

Submit your article to this journal ☑

View related articles ☑

View Crossmark data ☑

I·M3
Institute of Materials,
Minerals & Mining

Taylor & Francis
Taylor & Francis Group

Check for updates

Incorporating latent hardening in visco-plastic self-consistent framework for performing texture simulations

Mirtunjay Kumar[a], Amit Singh[a], Vikrant Kumar Beura[a] and Sumeet Mishra[b]

[a]Department of Materials Science and Engineering, Indian Institute of Technology Kanpur, Kanpur, India; [b]Department of Metallurgical and Materials Engineering, Indian Institute of Technology Roorkee, Roorkee, India

ABSTRACT

In the present work, the role of latent hardening on texture evolution at large strains is examined by embedding the latent hardening interaction matrix in the visco-plastic self-consistent framework. All possible interactions between different slip systems are allowed by specifying the 12 × 12 interaction matrix which consists of the relative strength of different dislocation junctions. In particular, the role of colinear junction which is the strongest among all dislocation locks on texture evolution is highlighted. It was observed that texture simulations in the latent hardening mode with a strong colinear lock provided excellent agreement with the experimentally measured textures, whereas isotropic hardening mode (12 × 12-unit matrix) failed to reproduce the experimental textures in a satisfactory manner.

Introduction

Over the years, several experimental and modelling studies have been carried out using the parabolic Taylor equation to understand dislocation-dislocation interaction and analyse the work hardening behaviour [1,2]. Considering a dislocation array of spacing l, Taylor showed that the stress (τ) required to move individual dislocation rows past each other is inversely proportional to l.

$$\tau = \frac{C}{l}(C = \text{constant}) \qquad (1)$$

Furthermore, the average dislocation density (ρ_{avg}) is related to spacing, l, as $\rho_{avg} = 1/l^2$. Therefore, Equation (1) can be rewritten as

$$\tau = C\sqrt{\rho_{avg}} \qquad (2)$$

The above equation has been hugely popular and is used widely across the research community for interpreting material response to the imposed deformation conditions [3–7]. Although the Taylor equation is relatively simple and can provide a quick prediction of the material deformation behaviour, it masks several crucial information such as the evolution of dislocation densities on individual slip systems and the type of dislocation junctions and their relative strength. Such detailed information about the material behaviour can only be obtained by specifying the latent hardening matrix (12 × 12; Table 2) and assigning appropriate strength to the different types of dislocation junctions [8,9]. The concept of latent hardening and

its subsequent influence on hardening behaviour and texture evolution are shown schematically in Figure 1. For tensile axis lying within the fundamental zone, slip on the primary system (111) [$\bar{1}$01] will rotate the tensile axis towards the primary slip direction [$\bar{1}$01]. However, as the tensile axis reaches the [001]–[$\bar{1}$11] boundary line, the conjugate slip system ($\bar{1}\bar{1}$1) [011] will also get activated and carry an equal amount of shear as that of the primary slip system [10]. As a result, the tensile axis will rotate towards [$\bar{1}$12], which is a stable orientation [10]. Nonetheless, such theoretical observations are rarely captured experimentally. Usually, the tensile axis overshoots by some finite angle into the conjugate triangle before the conjugate slip system ($\bar{1}\bar{1}$1) [011] becomes active [10]. This suggests that the critical stress required for slip on conjugate slip system must be higher than the primary slip system, which implies that slip on primary slip system latent hardens the conjugate slip system more than the active primary slip system.

This phenomenon of latent hardening affects the choice of slip systems and consequently the deformation texture and work hardening behaviour [11–14]. Both texture and work hardening are known to be the two key parameters which control the performance of a material in an actual industrial processing cycle. Therefore, it is of paramount importance to understand the role played by latent hardening on the selection of slip systems.
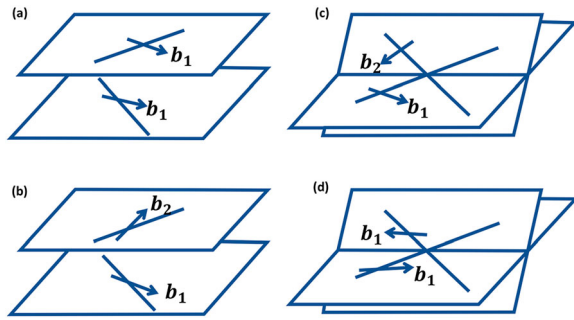
In this regard, Franciosi and Zaoui [15,16] have made a seminal contribution and performed the first
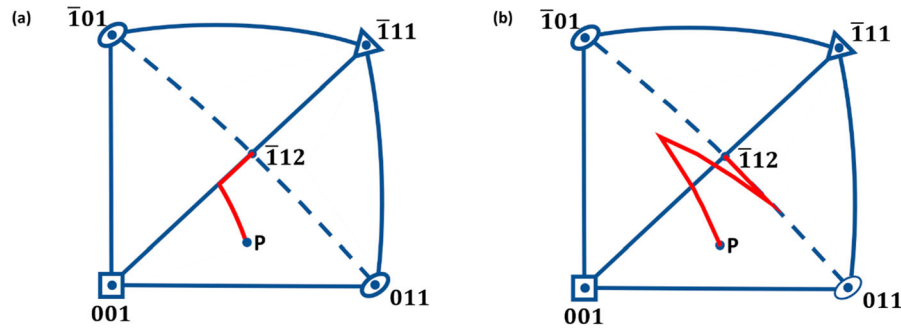
Figure 1. Schematic of rotation of tensile axis: (a) isotropic hardening and (b) latent hardening.

Figure 2. Schematic of different dislocation interactions: (a) self-locks, (b) coplanar locks, (c) attractive interactions between dislocations for Hirth lock, glissile lock and Lomer–Cottrell lock and (d) colinear lock.

Table 1. Nomenclature for the Schmid–Boas notation of 12 slip systems in f.c.c. materials.

Notation	A2	A3	A6	B2	B4	B5
n	$[\bar{1}11]$	$[\bar{1}11]$	$[\bar{1}11]$	$[111]$	$[111]$	$[111]$
b	$[0\bar{1}1]$	$[101]$	$[110]$	$[0\bar{1}1]$	$[\bar{1}01]$	$[\bar{1}10]$

Notation	C1	C3	C5	D1	D4	D6
n	$[\bar{1}\bar{1}1]$	$[\bar{1}\bar{1}1]$	$[\bar{1}\bar{1}1]$	$[1\bar{1}1]$	$[1\bar{1}1]$	$[1\bar{1}1]$
b	$[011]$	$[101]$	$[\bar{1}10]$	$[011]$	$[\bar{1}01]$	$[110]$

Table 2. Latent hardening interaction matrix for f.c.c. polycrystals.

	A2	A3	A6	B2	B4	B5	C1	C3	C5	D1	D4	D6
A2	a_0	a_1	a_1	a_3	a_4	a_4	a_2	a_4	a_5	a_2	a_5	a_4
A3	a_1	a_0	a_1	a_4	a_2	a_5	a_4	a_3	a_4	a_5	a_2	a_4
A6	a_1	a_1	a_0	a_4	a_5	a_2	a_5	a_4	a_2	a_4	a_4	a_3
B2	a_3	a_4	a_4	a_0	a_1	a_1	a_2	a_5	a_4	a_2	a_4	a_5
B4	a_4	a_2	a_5	a_1	a_0	a_1	a_5	a_2	a_4	a_4	a_3	a_4
B5	a_4	a_5	a_2	a_1	a_1	a_0	a_4	a_3	a_5	a_4	a_4	a_2
C1	a_2	a_4	a_5	a_2	a_5	a_4	a_0	a_1	a_1	a_3	a_4	a_4
C3	a_4	a_3	a_4	a_5	a_2	a_4	a_1	a_0	a_1	a_4	a_2	a_5
C5	a_5	a_4	a_2	a_4	a_4	a_3	a_1	a_1	a_0	a_4	a_5	a_2
D1	a_2	a_5	a_4	a_2	a_4	a_5	a_3	a_4	a_4	a_0	a_1	a_1
D4	a_5	a_2	a_4	a_4	a_3	a_4	a_4	a_2	a_5	a_1	a_0	a_1
D6	a_4	a_4	a_3	a_5	a_4	a_2	a_4	a_5	a_2	a_1	a_1	a_0

systematic experimental trial to determine the latent hardening matrix of aluminium and copper. Subsequently, dislocation dynamics (DD) simulations were performed by several groups such as Devincre et al. [17], Madec et al. [18] and Gerard et al. [19] to closely examine the interaction between slip systems and identify the different types of reaction products (dislocation junctions). The DD simulations have highlighted that there are six different types of dislocation junctions which can be categorised as self-locks (a_0), coplanar locks (a_1), Hirth locks (a_2), colinear locks (a_3), glissile locks (a_4) and Lomer–Cottrell locks (a_5) [17–19]. The different dislocations locks are shown schematically in Figure 2. The self-lock corresponds to interaction between dislocations belonging to same slip system. It is generally accepted to be a weak lock with minimal contribution towards hardening [20]. The coplanar lock corresponds to interaction between dislocations having the same slip plane. This lock is similar to the self-lock and contributes minimally towards hardening [20]. The Hirth lock corresponds to interaction between dislocations with perpendicular Burgers vector [20]. It is one of the three locks resulting from attractive interaction between dislocations and is generally considered to be the weakest among the three [21]. The other two locks resulting from attractive interactions are glissile and Lomer–Cottrell locks. These two locks are stronger compared to Hirth lock and are generally assigned the same strength [19,20]. Together, the

Hirth lock, Lomer–Cottrell lock and glissile lock constitute the forest type interaction [19,20]. The colinear lock corresponds to interaction between dislocations with parallel Burgers vector namely the slip plane of each dislocation is the cross-slip plane of the other. Over the years, the strength of colinear locks has courted significant controversy. Nonetheless, recent careful experimental and simulation works have clearly established that colinear locks are the strongest out of all the six different locks [18–20]. Table 2 summarises the different dislocation locks observed in f.c.c. materials based on Schmid and Boas notation for the slip systems (Table 1).

In order to analyse the effect of latent hardening on material deformation behaviour, the full 12×12 interaction matrix shown in Table 2 with appropriate strength of different dislocation locks has to be implemented in a crystal plasticity (CP) framework to perform texture and hardening simulations. Some well-accepted values regarding strength of dislocation locks are summarised in Table 3. In recent times, the interaction matrix has been used in a CP framework to predict the hardening behaviour during strain path

Table 3. Strength of dislocation locks obtained from DD simulations and experiments.

Parameter sets	a0	a1	a2	a3	a4	a5
Isotropic hardening	1	1	1	1	1	1
Fivel et al. [22]	0.01	0.4	0.4	0.4	0.75	1
Dumoulin et al. [23]	0.2	0.8	0.8	0.8	0.8	1
Tabourot et al. [24]	0.96	0.96	0.96	0.96	0.96	1
Madec et al. [18]	0.084	0.084	0.051	1.265	0.075	0.084
Devincre et al. [17]	0.122	0.122	0.07	0.625	0.137	0.122
Gérard et al. [19]	0.025	0.01	0.04	14.3	0.6	0.5

changes [25,26]. Depending upon the extent of strain path change such as orthogonal loading (cross loading) or full reversal, a transient in work hardening rate is generally observed. For other type of strain path changes in the major-minor strain space such as equibiaxial loading followed by uniaxial loading a permanent softening was observed by Iadicola et al. [25]. By including latent hardening on multiple slip systems, the decrease in flow stress and hardening rate upon change in strain path was successfully captured by CP models [25]. However, CP simulations for texture evolution at large strains have not been performed systematically by considering the full interaction matrix (Table 2). This has been partly due to increased computational cost of allowing latent hardening on all slip systems as well as the difficulties in determining the dislocation junction resistance in an accurate manner. Nonetheless, recent DD simulations have greatly facilitated determination of dislocation junction resistance in a fairly accurate manner [17,18]. Therefore, it is necessary to consider the physical phenomenon of latent hardening in CP and not avoid its existence in texture studies. It should be noted that in most of the previous works on texture simulations, latent hardening has been described by two independent coefficients [25]. It is generally assumed that all inactive slip systems harden in a similar manner. However, in the present work, we allow all possible interactions between different slip systems to develop a clear picture of the role of latent hardening on texture evolution.

In this regard, we have integrated the 12×12 interaction matrix with the visco-plastic self-consistent code developed by Lebensohn and Tome [27,28] and performed texture simulations to large rolling strains corresponding to 98% reduction in thickness. In order to carry out the present work, we have chosen silver (Ag) as a model material. The thought process behind choosing Ag was the latent hardening effects are more prevalent in low stacking fault energy (SFE) materials (Ag ~ 20 mJ m^{-2}) compared to medium and high SFE materials.

Materials and methods

Pure silver with 99.95% purity was used for performing the present work. The as-received samples were annealed at 723 K for one hour to remove any remnant traces of strain heterogeneity and obtain a fairly equiaxed grain microstructure. The annealed samples were then cut into blocks of dimensions 10 cm $\times$ 5 cm $\times$ 10 mm and subjected to rolling up to 98% reduction in thickness namely true strain of $\sim \varepsilon = -3.91$. Rolled samples were also retained after 50% ($\varepsilon = -0.69$), 75% ($\varepsilon = -1.4$) and 90% ($\varepsilon = -2.3$) reduction to comprehend the evolution of rolling texture in pure silver. The entire rolling schedule was carried out in an incremental manner with each step corresponding to a strain of -0.1. An X-ray goniometer equipped with alpha tilting ($\alpha = 0$–75°) and beta rotation ($\beta = 0$–360°) facility was used for determining the texture of rolled samples via measurement of four incomplete pole figures namely (111), (200), (220) and (311). It should be noted that pole figure measurements were done at the mid-thickness of the rolled samples (rolling direction-transverse direction plane) to avoid shear deformation effects due to friction between rolls and the sample surface. The criteria of plane strain conditions are only satisfied at the mid-thickness level. The experimentally measured incomplete pole figures were then imported into MTEX and subjected to defocussing and background corrections followed by ODF (orientation distribution function) estimation via harmonic series expansion method. Ghost correction was also employed during calculation of ODF's from the incomplete pole figures. The orthorhombic sample symmetry (twofold axis along RD, TD and ND) was imposed during computation of ODF's. In the present work, texture representation is done via ODF's by illustrating three main φ_2 sections namely 0°, 45°, 65°. This is a widely accepted practice in the texture community as all the typical rolling texture components can be identified in these three φ_2 sections.

MTEX is a freely available software package based on MATLAB for modelling and analysing crystallographic texture and microstructure, from the experimentally measured pole figure and/or EBSD data. MTEX does calculations through nonequispaced Fast Fourier Transformation (NFFT) algorithms (https://mtex-toolbox.github.io/index.html).

In the present study, the $L2$ loss function was applied to determine the minimised error between experimental and simulated textures. In general, it can be computed as per the following equation.

$$L2 \text{ Loss function} = \sum [f(g)_{\text{exp.}} - f(g)_{\text{sim.}}]^2 \quad (3)$$

where $f(g)_{\text{exp.}}$ and $f(g)_{\text{sim.}}$ are the function of orientation distributions in Euler space.

Visco-plastic self-consistent simulation (VPSC)

As mentioned in the introduction section, the 12×12 interaction matrix was integrated in the VPSC environment for performing texture simulations. Complete

details regarding VPSC code can be found in the manual developed by Tome and Lebensohn [27]. However, for the sake of completeness, a brief explanation of the visco-plastic slip and the self-consistent formulism is provided in the following paragraphs.

The visco-plastic slip is based on the rate-sensitive constitutive law [29] which can be expressed as

$$\tau_r^s = \tau_0^s \left(\frac{\dot{\gamma}_r^s}{\dot{\gamma}_r^0} \right)^m \tag{4}$$

Here, τ_r^s is the resolve shear stress on slip system 's', τ_0^s is the resolved shear stress related to reference shear rate value $\dot{\gamma}_r^0$ and $\dot{\gamma}_r^s$ is the shear rate on slip system 's'. The term 'm' is related to strain rate sensitivity. By inverting the above equation, we obtain,

$$\dot{\gamma}_r^s = \dot{\gamma}_r^0 \frac{\tau_r^s}{\tau_0^s} \left(\frac{\tau_r^s}{\tau_0^s} \right)^{\frac{1}{m}-1} \tag{5}$$

Equation (5) facilitates the calculation of shear rate on individual slip systems by projecting the stress tensor (σ) on the slip system.

$$\tau_r^s = \sigma : M^s, M^s = \frac{1}{2}(\vec{b}_i^s \vec{n}_j^s + \vec{b}_j^s \vec{n}_i^s) \tag{6}$$

Here, $\vec{b}$ and $\vec{n}$ are Burgers vector and slip plane normal, respectively. Equation (5) can now be rewritten as

$$\dot{\gamma}_r^s = \dot{\gamma}_r^0 \frac{\sigma : M^s}{\tau_0^s} \left(\frac{\sigma : M^s}{\tau_0^s} \right)^{\frac{1}{m}-1} \tag{7}$$
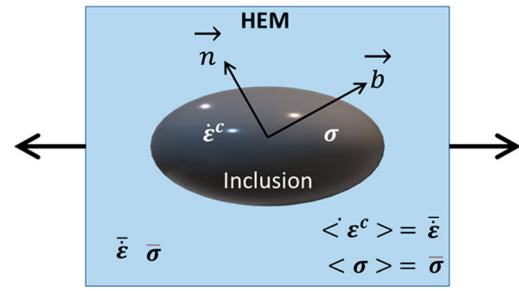
It should be noted that slip system resistance is represented by the parameter τ_0^s. The hardening of the material is usually simulated by increasing the τ_0^s value via the extended Voce equation.

$$\tau_0^s = \tau_i^s + (\tau_s^s + \theta_1^s \Gamma) \left[1 - \exp \left(-\frac{\theta_0^s \Gamma}{\tau_s^s} \right) \right] \tag{8}$$

Here, τ_i^s is the initial critical resolved shear stress (CRSS), θ_0^s is the initial hardening rate, τ_s^s is the back extrapolated CRSS and θ_1^s is the asymptotic hardening rate. In the present work the Voce hardening parameters were taken from the classical works of Beyerlein et al. [30] (Table 4).

The self-consistent formulism is based on the fact that the shape of the grain can be taken into account during simulations by considering the interaction of the grain with its surrounding homogenous equivalent medium (Figure 3). This interaction is typically expressed by the following equation.

$$\dot{\varepsilon}^c - \bar{\bar{\varepsilon}} = \mathrm{n}^{\mathrm{eff}} (I - E)^{-1} : E : \bar{M} : (\sigma - \bar{\sigma}) \tag{9}$$

Table 4. Voce hardening parameters (MPa).

τ_0	τ_1	θ_0	θ_1
33	38	65	2

Figure 3. Schematic of the VPSC formalism where an inclusion is embedded in a homogenous equivalent medium (HEM).

Here, $\dot{\varepsilon}^c$ and σ are the local strain rate and stress inside the grain, $\bar{\bar{\varepsilon}}$ and $\bar{\sigma}$ are the average macroscopic strain rate and stress, I is the identity tensor, E is the Eshelby tensor, $\bar{M}$ is the macroscopic compliance modulus and n^{eff} is the grain level linearisation parameter. For $n^{\mathrm{eff}} = 0$, upper bound Taylor conditions are approached, while $n^{\mathrm{eff}} = \infty$ results in the static model. Other interaction schemes with different values of n^{eff} such as 1, 10 and 20 are also supported in the VPSC source code. In the present work, we have used $n^{\mathrm{eff}} = 20$ for performing texture simulations as it is generally considered to be suitable for mimicking deformation conditions in low SFE f.c.c. materials [31].

Results

The initial texture and microstructure (inverse pole figure map obtained from EBSD) of the annealed samples prior to rolling is shown in Figure 4. It can be observed that the initial texture approaches a nearly random distribution with maximum intensity of 1.5 m.r.d. The microstructure can be characterised by the presence of large strain free and equiaxed grains.

The measured rolling texture after different thickness reductions are shown in Figure 5 in terms of ODF in the Euler space for the three different φ_2 sections. Upon comparing with the starting material which had a nearly random texture, it can be observed that rolled samples develop a relatively stronger texture with maximum intensity reaching 5.1 m.r.d after 98% thickness reduction. The ideal orientations such as $\{110\}\langle 001 \rangle$ Goss (G) and $\{110\}\langle 1\bar{1}2 \rangle$ Brass (Bs) which characterise the deformation texture of the rolled silver sheets are marked in the $\varphi_2 = 0°$ and $\varphi_2 = 45°$ sections to facilitate texture interpretation. In addition, the alpha fibre which extends from Goss to rotated Goss (R.G.) position via the Brass component is also marked ($\varphi_1 = 0 - 90°, \varphi = 45°, \varphi_2 = 0°$). It can be observed that after 50% reduction, the maximum texture intensity is near the Goss position. However, with increasing rolling reduction, the texture intensity spreads along the alpha fibre with nearly equal intensity at Goss and Brass position after 98% rolling reduction. It should be noted that there is a complete absence of other characteristic
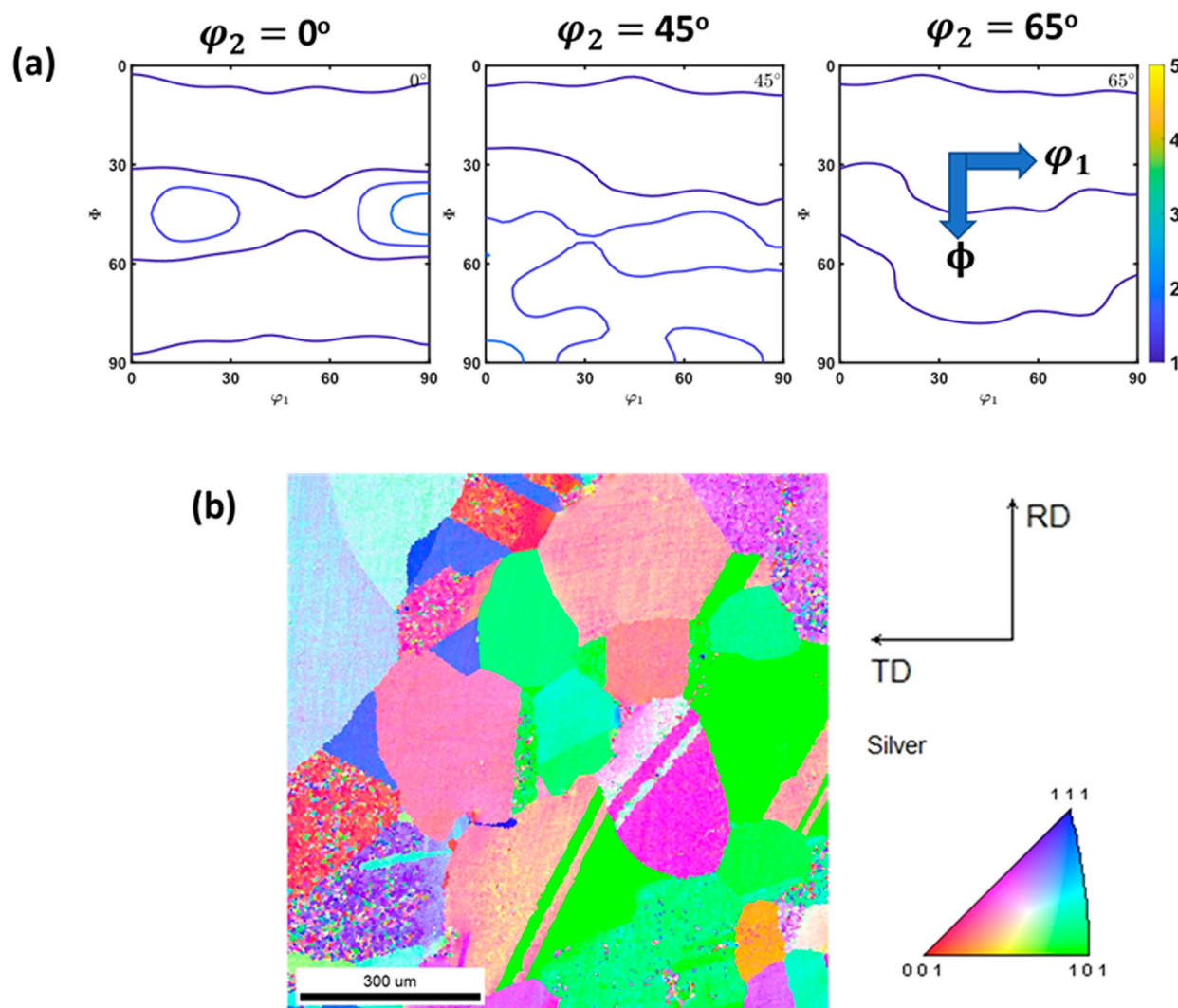
Figure 4. Initial (a) texture and (b) microstructure of the annealed samples.

texture components such {112}⟨11$\bar{1}$⟩ Copper (Cu) and {123}⟨63$\bar{4}$⟩ S throughout the entire rolling deformation. Therefore, it can be said that the rolling texture evolution in silver falls in the domain of the well-known 'Brass type texture' which is typically observed in low SFE materials [32,33]. Over the years, the evolution of Brass type texture (combination of Brass and Goss components) has been a much debatable topic in the texture community and several mechanisms have been proposed to explain this texture evolution [32]. Nonetheless, a common consensus among researchers is yet to be achieved.

The first theory in this regard was based on the higher propensity of twinning in {112}⟨11$\bar{1}$⟩ Copper oriented grains which would cause rotation of the Copper component towards {552}⟨11$\bar{5}$⟩ Copper twin orientation, which will subsequently rotate towards Goss/Brass position via octahedral slip [34]. Nonetheless, this theory has now been discarded as there is ample evidence which suggests that volume fraction of twins in a rolled microstructure is not enough to cause such drastic changes in texture. Another school of thought was also related to the role of twinning on

Brass type texture evolution, although in an indirect manner. Leffers et al. [35,36] argued that twinning in the initial stages of deformation would result in strong hindrance of slip on non-coplanar systems. As a result, the propensity for planar slip will be accentuated which in turn would result in development of Brass type texture. However, texture simulations in the planar slip framework predict an excessively strong Brass component along with an incomplete alpha fibre, which is in contrast with experimental results where a well-developed alpha fibre with prominent Goss and Brass component is generally observed after large rolling reductions. Moreover, the modified Sachs model proposed by Leffers et al. [37] to consider the indirect of twinning on enhancing planar slip has not found widespread use in the texture community. Other mechanisms such as slip on non-octahedral slip systems and partial slip via ⟨11$\bar{2}$⟩ dislocations have also been proposed to explain the evolution of Brass type texture [38,39]. Nevertheless, conclusive microstructural evidence of slip traces on non-octahedral planes and presence of stacking faults due to partial slip is lacking in literature. In recent times, with the advent of electron back
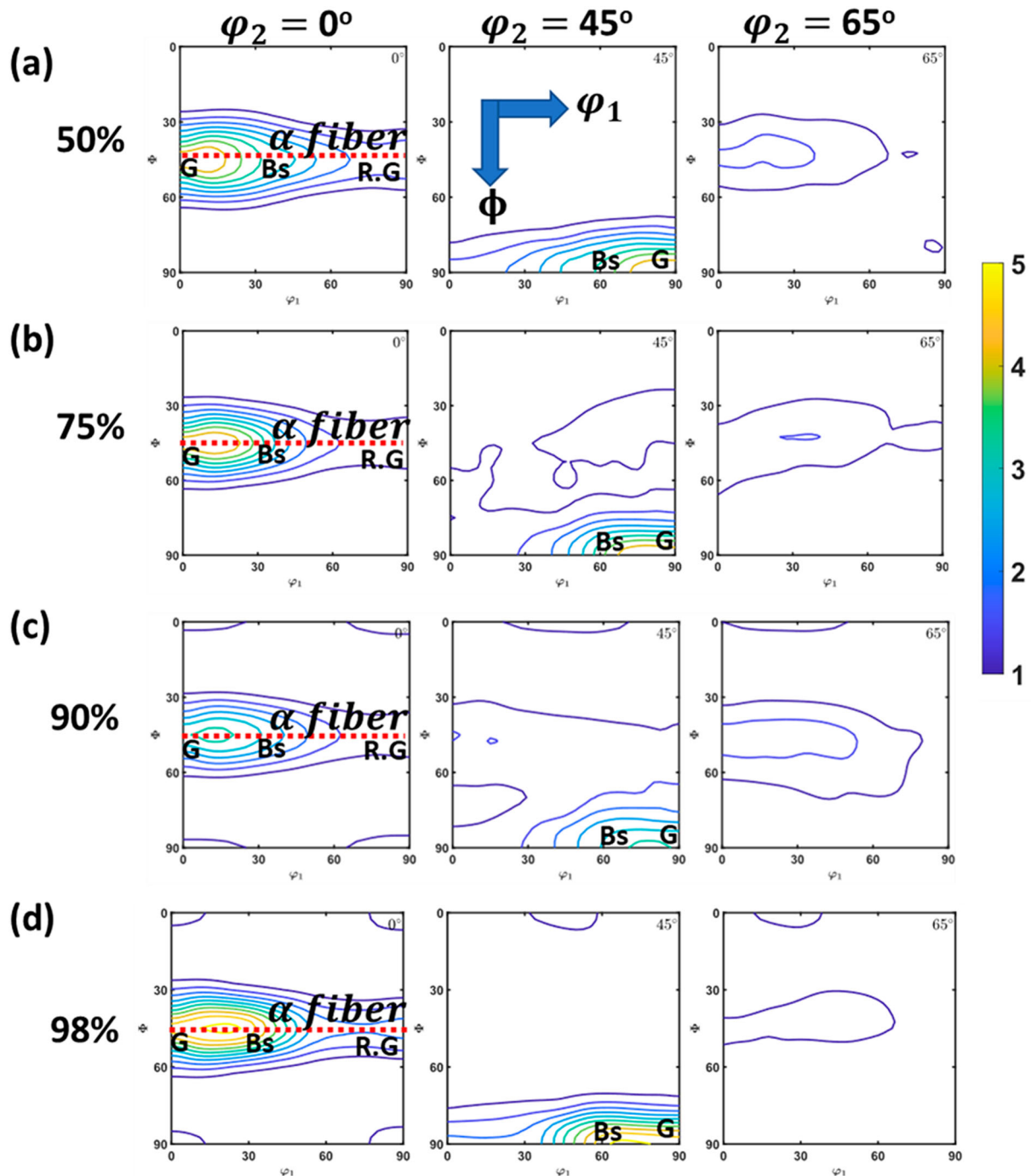
Figure 5. Important sections of the ODF after different rolling reductions: (a) 50%, (b) 75%, (c) 90% and (d) 98%.

scatter diffraction, several researchers have highlighted the possible role of shear bands in causing the evolution of Brass type texture [40,41]. However, it should be noted that shear bands are generally observed at relatively large rolling reductions, whereas the evolution of Brass type texture is characteristically different from Copper type texture (combination of Copper, S and relatively weak Brass component) from the early stages of deformation [36].

Apart from the above-mentioned mechanisms, one particular theory in the framework of thermally activated dislocation motion namely 'cross-slip' has found relatively higher acceptance among researchers in the texture community. Based on the experimental results

regarding the effect of temperature and strain rate on the evolution of rolling texture, parallelisms have been drawn between restricted cross slip and the evolution of Brass type texture [42,43]. However, till date the propensity of cross slip has not been explicitly integrated in a CP model for performing texture simulations. There have been some attempts where cross-slip functions have been introduced in the CP environment in an empirical manner to control the amount of cross slip and thereby simulate the different types of rolling textures [44]. In this regard, the present work concerned with dislocation junctions, their relative strengths and latent hardening offers great flexibility as the propensity of cross slip can be simply
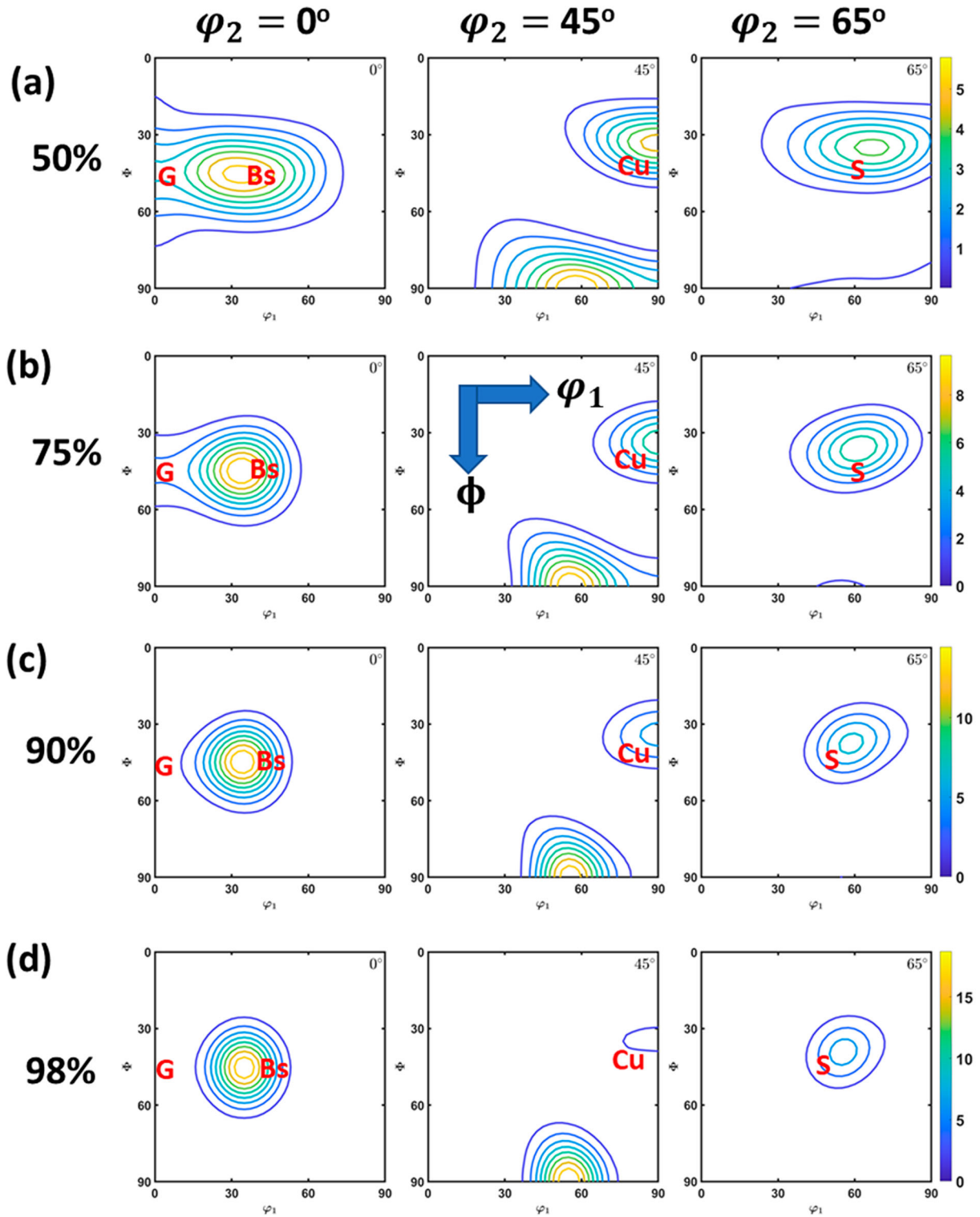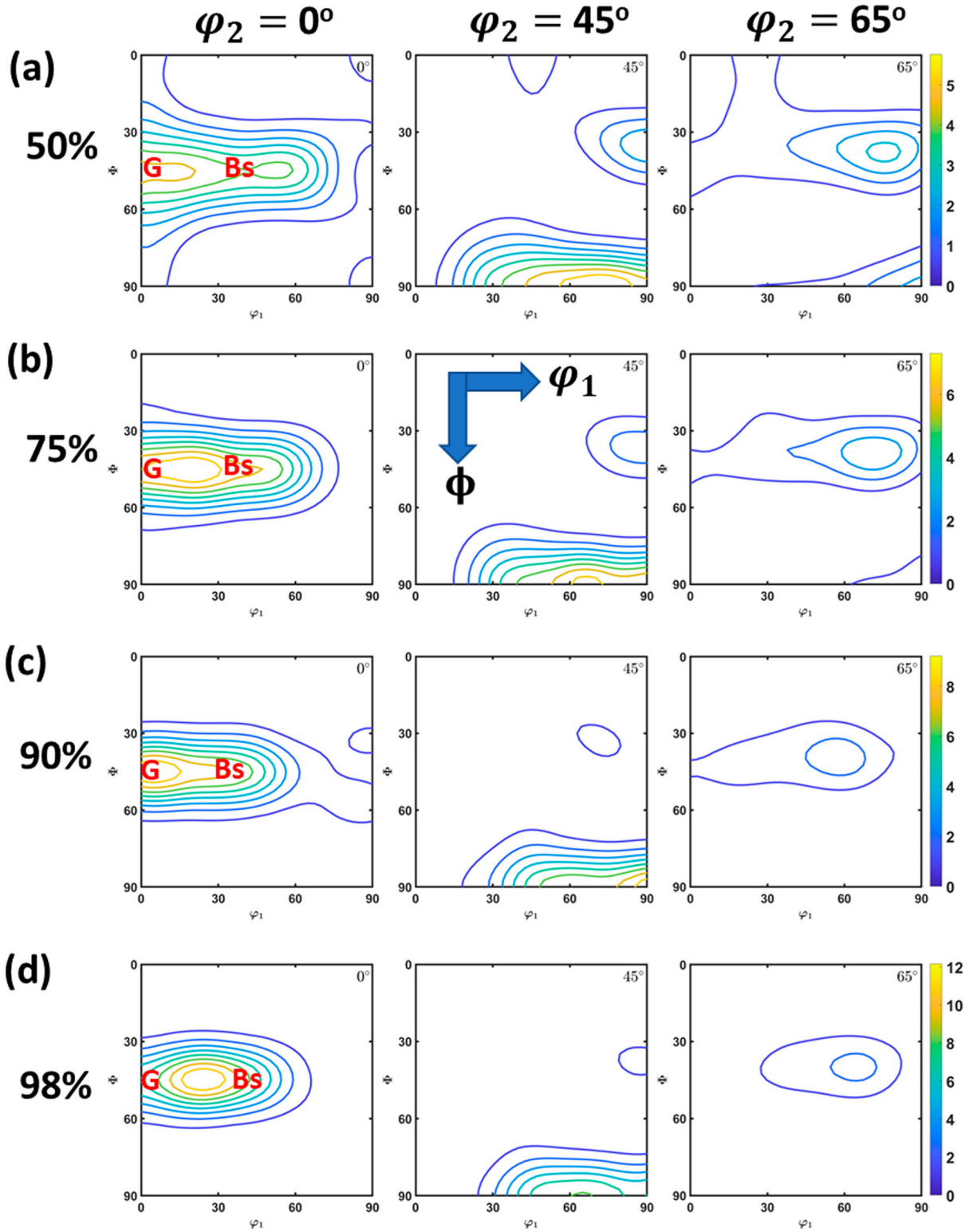
Figure 6. Simulated textures obtained from VPSC assuming isotropic hardening: (a) 50%, (b) 75%, (c) 90% and (d) 98%.

controlled by specifying the strength of colinear locks (Tables 2 and 3).

To illustrate our argument, we have performed VPSC simulations using two different interaction matrices namely corresponding to isotropic hardening and the coefficients suggested by Gérard et al. [19] (Table 3). As mentioned previously in the introduction section, systematic experimental trials involving several changes in strain path were carried out by Gérard et al. [19] to arrive at the interaction matrix. A

closer examination of the coefficients derived by Gérard et al. [19] highlights a very important point regarding the strength of colinear locks which is significantly stronger compared to other dislocation junctions. Similar remarks regarding the strength of colinear locks were also made by Devincre et al. [17] and Madec et al. [18] at the turn of the century via DD simulations. The relatively high values for colinear locks will restrict the amount of cross slip, which in turn will have significant implications on the evolution of texture during rolling

Figure 7. Simulated textures obtained from VPSC assuming latent hardening: (a) 50%, (b) 75%, (c) 90% and (d) 98%.

deformation [42,43]. In the following paragraphs the simulation results obtained from the two different sets of interaction matrices are illustrated and the advantages of considering the role of latent hardening in CP studies are outlined.

For performing VPSC simulations, the starting texture (Figure 4) was discretized to obtain 10000 single orientations, which were then used as input in the VPSC code. The MATLAB code based on MTEX

for performing discretization is provided in the supplementary file. The velocity gradient (L_{ij}) which was imposed for mimicking rolling deformation was:

$$L_{ij} = \begin{bmatrix} L_{11} & 0 & 0 \\ 0 & 0 & 0 \\ 0 & 0 & L_{33} \end{bmatrix} \tag{10}$$

Here, $L_{11} = -L_{33}$ for plane strain deformation. The simulations were performed in an incremental manner
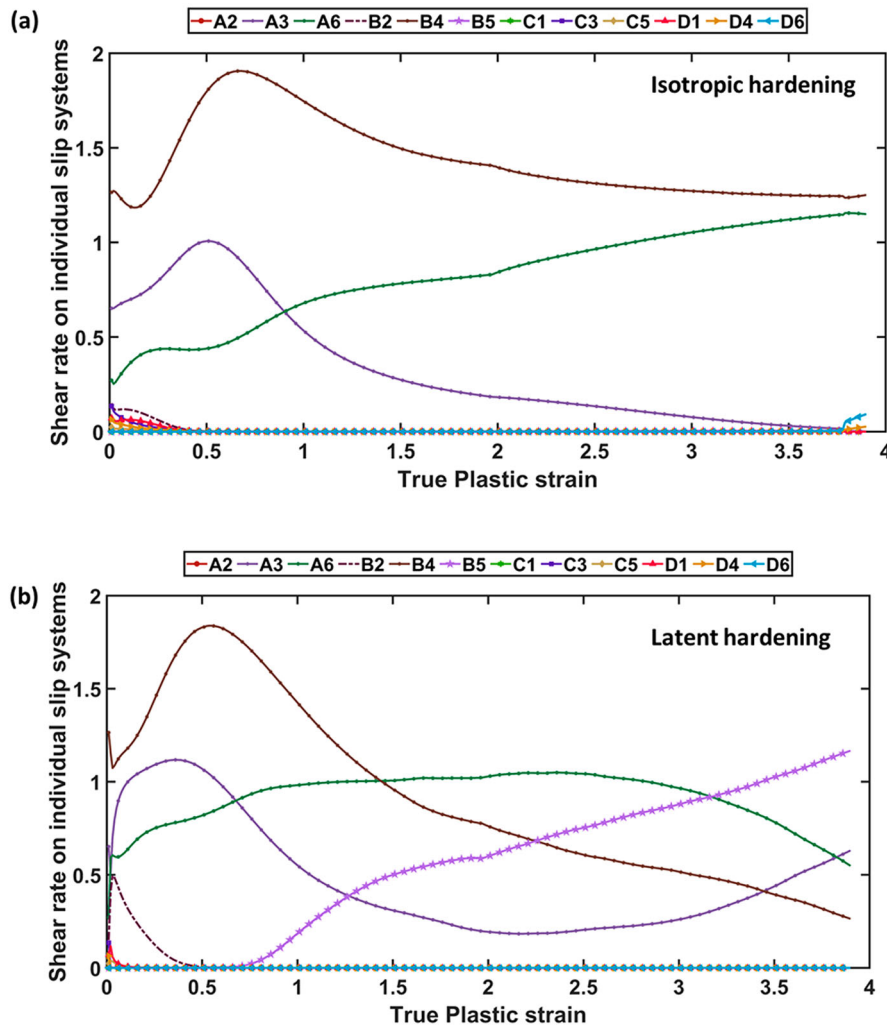
Figure 8. Evolution of shear rates on 12 individual slip systems considering: (a) isotropic hardening and (b) latent hardening.

with each step corresponding to a strain increment of 0.01. In total, 391 steps were performed to achieve a cumulative strain of −3.91, which corresponds to 98% reduction in thickness. Texture outputs corresponding to 50% ($\varepsilon = -0.69$), 75% ($\varepsilon = -1.4$) and 90% ($\varepsilon = -2.3$) reduction in thickness were also stored to facilitate comparison with experimental textures. The simulations were performed using the tangent interaction scheme ($n^{\text{eff}} = 20$) which is widely accepted in the texture community for low SFE materials [31].

Figure 6 shows the simulated ODF sections corresponding to isotropic hardening. It can be clearly observed that isotropic hardening leads to considerable discrepancies between experimental and simulated textures at all levels of strain. At low to intermediate thickness reductions (50% and 75%), assumption of isotropic hardening leads to development of a prominent Copper (Cu) and S component which is not observed experimentally. On the other hand, at higher rolling reductions (90% and 98%), isotropic hardening predicts a strong Brass component and an incomplete alpha fibre, which is contrast with the experimental results.

Figure 7 shows the simulation results corresponding to latent hardening based on the coefficients derived

by Gérard et al. [19]. A visual evaluation suggests that proximity between experimental and simulated textures is greatly enhanced by considering the latent hardening matrix in the VPSC environment. The main texture characteristics of a well-developed alpha fibre along with spread of intensity between Goss and Brass components is satisfactorily captured for all stages of rolling deformation. The difference between the experimental and simulated ODF sections is shown in Figure 9. It can be observed that error between the ODF's is always higher for isotropic hardening compared to latent hardening. Hence, the pressing need of considering latent hardening in texture simulations can be clearly established from the results shown in Figures 7 and 9.

Discussion

Such marked differences in texture between isotropic and latent hardening can be better understood by examining the evolution of shear rates on individual slip systems as well the average number of active slip systems (AVACS) during rolling deformation. The evolution of shear rates on each of the 12 slip systems and
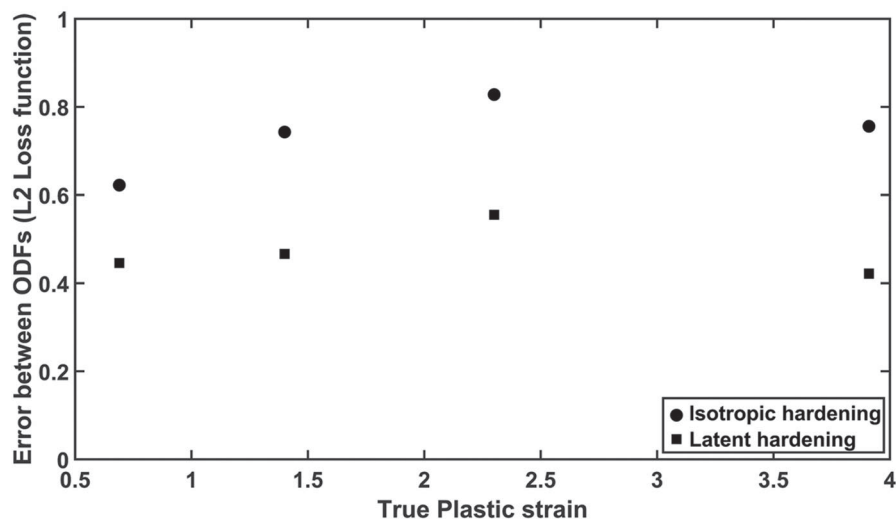
Figure 9. Comparison of the difference between experimental and simulated ODF's based on isotropic and latent hardening.

AVACS are shown in Figures 8 and 10, respectively. Both the shear rate and AVACS plot suggest that there are ∼ 2–2.5 slip systems (A6, B4 (Table 1)) which carry majority of the total shear in case of isotropic hardening, whereas multiple slip systems (∼ 3.5) are active when latent hardening is considered for texture simulations. It is well known that when dislocation glide is restricted to few slip systems, Sachs type deformation pattern is approached which results in evolution of a single dominating Brass component. Moreover, the strain compatibility requirements at the grain boundaries are also violated in the Sachs type deformation mode. On the other hand, relatively higher number of active slip systems (> 3) as predicted by the latent hardening interaction matrix is more apt for describing deformation behaviour of Ag w.r.t. strain compatibility. In addition, the experimentally observed feature of a complete alpha fibre with intensity spread between Goss and Brass position (Figures 5 and 7) is also predicted in a satisfactory manner by considering latent hardening parameters.

The insights obtained from the present work further confirms the hypothesis suggested by Leffers and Ray [32] and several other authors [31] that latent hardening is the most probable explanation of Brass type texture evolution in low SFE materials. The micromechanism by which latent hardening contributes towards Brass type texture is by retarding the cross-slip propensity. The high value of colinear lock (a_3) obtained by DD simulations plays a key role in reducing the shear rates on cross-slip systems. To our best knowledge, very little amount of careful experiments and DD simulations have been performed over the years to evaluate the strength of the different dislocation junctions which are required to specify the 12×12 interaction matrix. In addition, whatever literature is there, it is mostly related to aluminium and copper [15,19,20]. In the absence of latent hardening

parameters for low SFE materials such as Ag, we used a 'very simplistic' assumption of using the latent hardening parameters obtained by Gérard et al. for copper [19]. Nonetheless, even with such a simplistic assumption, much better agreement with experimental texture is obtained by including latent hardening parameters in texture simulations compared to the standard practice of performing VPSC simulations in tangent interaction scheme with isotropic hardening. Further improvements w.r.t. texture simulations can be made by using the exact latent hardening parameters of Ag. In our future works, we aim to determine the values of six different dislocation locks by performing careful single-crystal experiments as well as DD simulations. Nonetheless, the trend w.r.t. strength of different locks will still remain the same. The colinear dislocation locks will be the strongest compared to other dislocation locks. Although, their absolute values might change with SFE. With new alloys being continuously developed which have even lower SFE compared to Ag, tuning of latent hardening parameters, especially the colinear lock a_3 will allow performing successful texture simulations.

The role of latent hardening is also important w.r.t. texture simulations of medium to high SFE materials. To illustrate our argument, we have performed texture simulations for cold-rolled copper (medium SFE ∼ 70 mJ m^{-2}) which is known to develop a characteristic Copper type texture after 95% rolling reduction. Considering that medium and high SFE materials tend to deform in close proximity with upper bound Taylor model, secant interaction scheme ($n_{\text{eff}} = 1$) was chosen for VPSC simulations. The simulations were performed in the framework of both isotropic and latent hardening (Gérard et al. [19]). A random texture was used as input for performing simulations up to a strain of $\varepsilon = -2.99$. The simulation results are shown in Figure 11. It can be clearly observed that isotropic
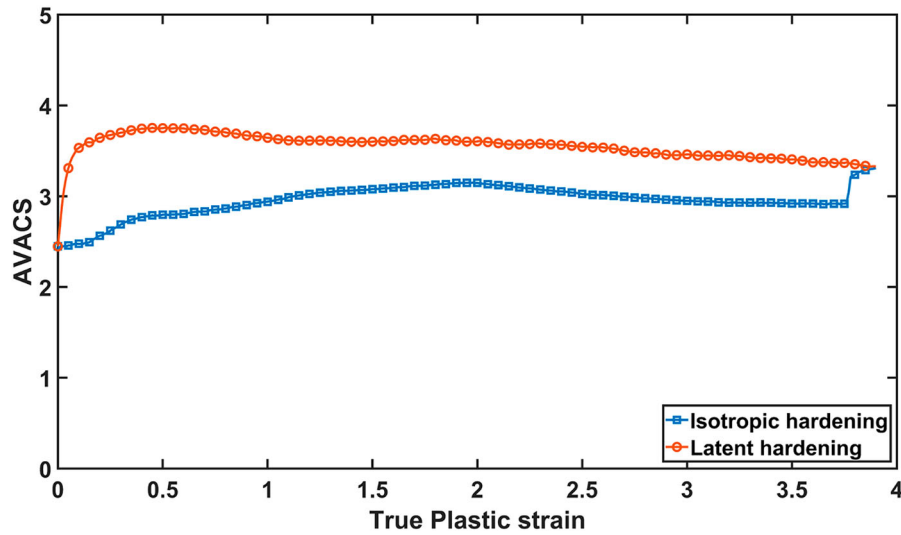
Figure 10. AVACS versus true plastic strain for isotropic and latent hardening.
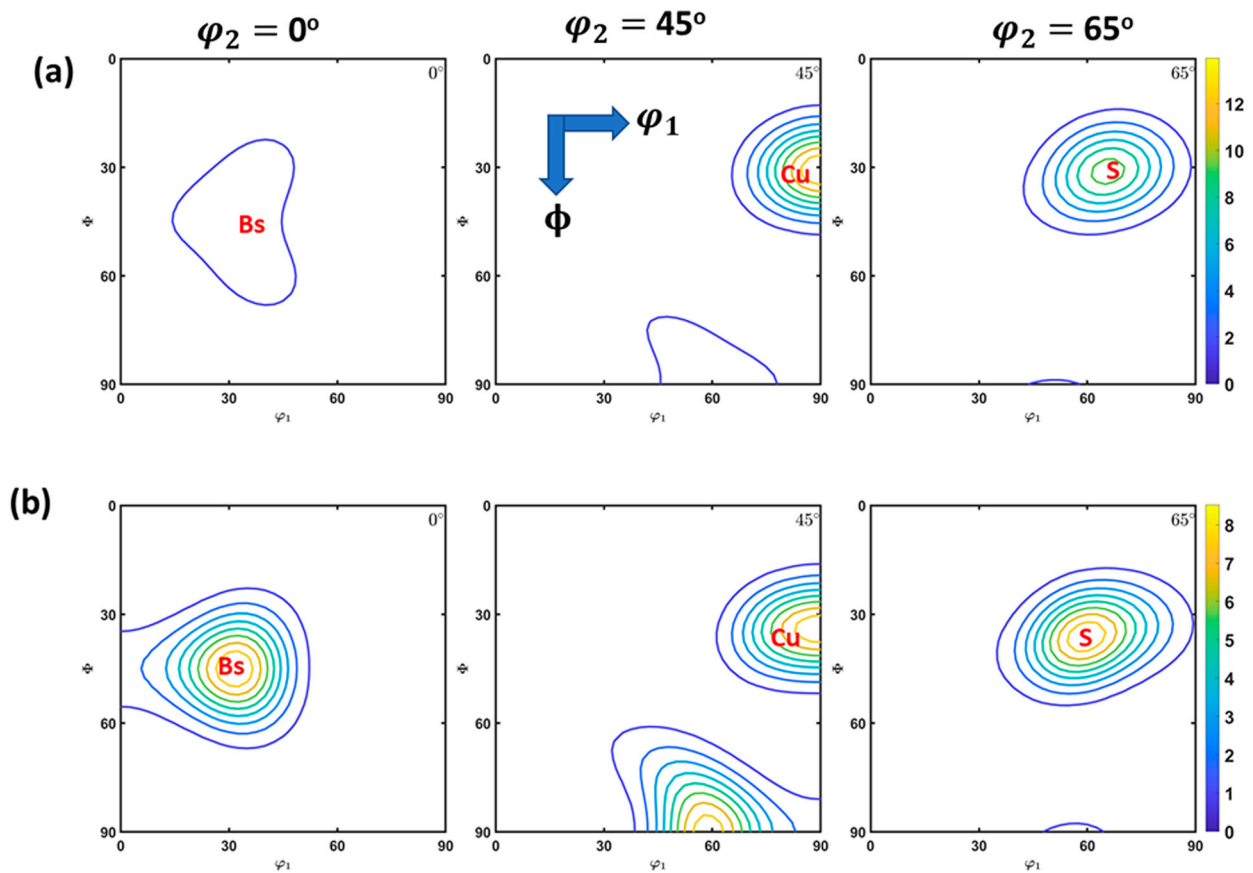
Figure 11. Simulated ODF sections after 95% rolling of copper obtained via VPSC (secant interaction scheme) for an initial random texture: (a) isotropic hardening and (b) latent hardening.

hardening causes development of strong Copper and S components with only a negligible intensity at Brass position. On the other hand, latent hardening results in development of a well-defined β fibre with intensity distributed at Copper, S and Brass positions. On comparison with experimental texture reported in Fig. 2 of Reference [32], it can be said that latent hardening provides a much better agreement with experimental texture compared to isotropic hardening. Therefore, it can be concluded that latent hardening in terms of

specifying the 12×12 interaction matrix should be considered for performing texture simulations. In this regard, careful and niche experiments are required to obtain the latent hardening parameters as a function of SFE.

Conclusions

The rationale for considering latent hardening interaction matrix during rolling texture simulation was

discussed in the present work. It was found that when interaction matrix with accurate description of different dislocation junctions is embedded in the VPSC environment, the experimental textures can be satisfactorily reproduced via VPSC simulations. The other important findings are summarised below:

(i) The evolution of shear rate on each of the 12 individual slip systems as well as the AVACS plot suggests that higher number of slip systems are active in the latent hardening mode compared to isotropic hardening.

(ii) The isotropic hardening mode approaches a Sachs type deformation mode which will lead to violation of strain compatibility across grain boundaries. On the other hand, higher number of active slip systems in latent hardening mode will permit accommodation of any arbitrary shape change and hence maintain strain compatibility.

(iii) The isotropic hardening mode predicts an incomplete alpha fibre with a strong Brass component, whereas a complete alpha fibre with well-defined Goss and Brass components is achieved in the latent hardening mode.

(iv) The new protocol of considering the interaction matrix in the VPSC environment allows to bridge the gap between DD simulations and CP simulations. Key insights regarding strength of different dislocation junctions from DD simulations can now be implemented in the CP codes.

Acknowledgements

Disclosure statement

References

[1] Taylor GI. The mechanism of plastic deformation of crystals. Part I. —theoretical. Proc Royal Soc A Math Phys Eng Sci. 1934;145(855):362–387.

[2] Taylor GI. The mechanism of plastic deformation of crystals. Part II.—comparison with observations. Proc Royal Soc A Math Phys Eng Sci. 1934;145(855):388–404.

[3] Saimoto S, Van Houtte P. Constitutive relation based on Taylor slip analysis to replicate work-hardening evolution. Acta Mater. 2011;59(2):602–612.

[4] Schouwenaars R. A statistical analysis of strain hardening: the percolation limit and the Taylor equation. Acta Mater. 2012;60(18):6331–6340.

[5] Ashby M. Work hardening of dispersion-hardened crystals. Philos Mag. 1966;14(132):1157–1178.

[6] Sevillano JG, Van Houtte P, Aernoudt E. Large strain work hardening and textures. Prog Mater Sci. 1980;25(2-4):69–134.

[7] Thompson AW, Baskes MI, Flanagan WF. The dependence of polycrystal work hardening on grain size. Acta Metall. 1973;21(7):1017–1028.

[8] Kubin L, Devincre B, Hoc T. Toward a physical model for strain hardening in fcc crystals. Mater Sci Eng A. 2008;483-484:19–24.

[9] Kubin L, Devincre B, Hoc T. Modeling dislocation storage rates and mean free paths in face-centered cubic crystals. Acta Mater. 2008;56(20):6040–6049.

[10] Hosford WF. The mechanics of crystals and textured polycrystals. New York: Oxford University Press; 1993. p. 248.

[11] Pham MS, Creuziger A, Iadicola M, et al. Roles of texture and latent hardening on plastic anisotropy of face-centered-cubic materials during multi-axial loading. J Mech Phys Solids. 2017;99:50–69.

[12] Hu H, Penelle R. On the influence of latent hardening on texture development in face-centered-cubic metals. Scr Metall Mater. 1991;25(2):377–382.

[13] Zecevic M, Knezevic M. Latent hardening within the elasto-plastic self-consistent polycrystal homogenization to enable the prediction of anisotropy of AA6022-T4 sheets. Int J Plast. 2018;105:141–163.

[14] Xie Q, Van Bael A, An YG, et al. Effects of the isotropic and anisotropic hardening within each grain on the evolution of the flow stress, the r-value and the deformation texture of tensile tests for AA6016 sheets. Mater Sci Eng A. 2018;721:154–164.

[15] Franciosi P, Berveiller M, Zaoui A. Latent hardening in copper and aluminium single crystals. Acta Metall. 1980;28(3):273–283.

[16] Franciosi P, Zaoui A. Multislip in fcc crystals a theoretical approach compared with experimental data. Acta Metall. 1982;30(8):1627–1637.

[17] Devincre B, Hoc T, Kubin L. Dislocation mean free paths and strain hardening of crystals. Science. 2008;320(5884):1745–1748.

[18] Madec R, Devincre B, Kubin L, et al. The role of collinear interaction in dislocation-induced hardening. Science. 2003;301(5641):1879–1882.

[19] Gérard C, Cailletaud G, Bacroix B. Modeling of latent hardening produced by complex loading paths in FCC alloys. Int J Plast. 2013;42:194–212.

[20] Khadyko M, Dumoulin S, Cailletaud G, et al. Latent hardening and plastic anisotropy evolution in AA6060 aluminium alloy. Int J Plast. 2016;76:51–74.

[21] Kubin L. Dislocations, mesoscale simulations and plastic flow. Vol. 5. Croydon: Oxford University Press; 2013.

[22] Fivel M, Tabourot L, Rauch E, et al. Identification through mesoscopic simulations of macroscopic parameters of physically based constitutive equations for the plastic behaviour of fcc single crystats. Le Journal de Physique IV. 1998;8(PR8):Pr8-151–Pr8-158.

[23] Dumoulin S, Tabourot L, Gradel T, et al. Identification of constitutive laws for Al 99.5. Adv Mech Behav Plast Damage Proc Euromat. 2000;2000:311.

[24] Tabourot L, Dumoulin S, Balland P. An attempt for a unified description from dislocation dynamics to metallic plastic behaviour. Le Journal de Physique IV. 2001;11(PR5):Pr5-111–Pr5-118.

[25] Iadicola MA, Hu L, Rollett AD, et al. Crystal plasticity analysis of constitutive behavior of 5754 aluminum sheet deformed along bi-linear strain paths. Int J Solids Struct. 2012;49(25):3507–3516.

[26] Pham M-S, Iadicola M, Creuziger A, et al. Thermally-activated constitutive model including dislocation

interactions, aging and recovery for strain path dependence of solid solution strengthened alloys: application to AA5754-O. Int J Plast. 2015;75:226–243.

[27] Tomé C, Lebensohn R. VPSC 7b – user manual. Los Alamos: U.S. Department of Energy (DOE); 2007.

[28] Tomé CN, Necker CT, Lebensohn RA. Mechanical anisotropy and grain interaction in recrystallized aluminum. Metall Mater Trans A. 2002;33(8):2635–2648.

[29] Zhou Y, Neale KW, Tóth LS. A modified model for simulating latent hardening during the plastic deformation of rate-dependent FCC polycrystals. Int J Plast. 1993;9(8):961–978.

[30] Beyerlein I, Toth LS, Tomé C, et al. Role of twinning on texture evolution of silver during equal channel angular extrusion. Philos Mag. 2007;87(6):885–906.

[31] Saleh AA, Haase C, Pereloma EV, et al. On the evolution and modelling of brass-type texture in cold-rolled twinning-induced plasticity steel. Acta Mater. 2014;70:259–271.

[32] Leffers T, Ray RK. The brass-type texture and its deviation from the copper-type texture. Prog Mater Sci. 2009;54(3):351–396.

[33] Hirsch J, Lücke K. Overview no. 76: mechanism of deformation and development of rolling textures in polycrystalline f.c.c. metals—I. Description of rolling texture development in homogeneous CuZn alloys. Acta Metall. 1988;36(11):2863–2882.

[34] Wassermann G. The influence of mechanical twinning on the formation of the texture in cubic metals. Z Metallkd. 1963;54(2):61.

[35] Leffers T. On the development of the brass-type texture. Texture Stress Microstruct. 1993;22(1):53–58.

[36] Leffers T, Jensen DJ. The early stages of the development of rolling texture in copper and brass. Texture Stress Microstruct. 1988;8:467–480.

[37] Leffers T. A modified Sachs approach to the plastic deformation of polycrystals as a realistic alternative to the Taylor model. In P. Haasen V. Gerold G. (eds) 5th International Conference on Strength of Metals and Alloys. Aachen: Pergamon Press; 1979.

[38] Hu H, Cline R, Goodman S. Deformation textures of metals. In H. Margolin (eds) Recrystallization, grain growth and textures. Ohio: ASM, Metals Park. 1966. p. 295–374.

[39] Maurice C, Driver J. Hot rolling textures of fcc metals—part I. Experimental results on Al single and polycrystals. Acta Mater. 1997;45(11):4627–4638.

[40] Madhavan R, Ray RK, Suwas S. New insights into the development of microstructure and deformation texture in nickel–60wt.% cobalt alloy. Acta Mater. 2014;78:222–235.

[41] Madhavan R, Ray RK, Suwas S. Texture transition in cold-rolled nickel–40wt.% cobalt alloy. Acta Mater. 2014;74:151–164.

[42] Leffers T. Deformation rate dependence of rolling texture in brass containing 5% zinc. Scr Metall. 1968;2(8):447–452.

[43] Leffers T, Pedersen OB. The activation energy for the fcc rolling-texture transition as related to the activation energy for cross slip. Scr Mater. 2002;46(10):741–746.

[44] Gangli P, Arató P. Computer simulation study of the role of cross-slip in the formation of textures in fcc metals. Philos Mag. 1976;34(3):465–478.